Electrochimica Acta 329 (2020) 135158

Contents lists available at ScienceDirect

Electrochimica Acta

journal homepage: www.elsevier.com/locate/electacta

Microstructure and electrochemical properties of IrO_2+RhO_x+ZrO_2 coated titanium anodes

R. Alibek, M. Atapour*, A. Aghajani, R. Ashari

Department of Materials Engineering, Isfahan University of Technology, Isfahan 84156-83111, Iran

ARTICLE INFO

Article history:
Received 5 May 2019
Received in revised form
22 October 2019
Accepted 25 October 2019
Available online 31 October 2019

Keywords:
Ti/(IrO_2+RhO_x+ZrO_2) anodes
Electro-catalytic activity
Electrical conductivity
Electrochemical stability
Oxygen evolution

ABSTRACT

The electrodes of Ti/IrO_2+RhO_x + ZrO_2 were prepared with varying proportions of RhO_x using thermal decomposition treatment at 550 °C. The microstructure of these coatings was investigated by SEM and XRD methods. The electrochemical behavior of coatings was assessed through accelerated life test (ALT), electrochemical impedance spectroscopy (EIS) and cyclic voltammetry (CV). The results showed that increasing the RhO_x content led to superior service lifetime and lower electrical conductivity of the coatings. Also, the results of cyclic voltammetry tests confirmed that the anodic voltammetric charge was enhanced by increasing the concentration of RhO_x in coatings. The EIS examination of the coatings indicated that the charge transfer resistance at the external active surface of the coatings was increased by adding the RhO_x content. Furthermore, it was found that the formation of TiO_2 passive layer at the interface of the substrate/oxides layer was the main destruction mechanism of the coated anodes. Among the tested anodes, the anode with 10%IrO_2-60%RhO_x-30%ZrO_2 coating exhibited larger electrochemically active surface area, higher stability and inferior electrocatalytic activity for oxygen evolution.

1. Introduction

Titanium substrates coated with mixed metal oxides (MMOs) are widely used as anodes in different electrochemical processes like electroplating, chloral alkali industries, electro-winning of metals, sewage treatment, oxidation of organics, and organic synthesis. Titanium electrodes coated with MMOs also named dimensionally stable anodes (DSAs) have shown advantages for use in cathodic protection [1–7]. Depending on the substrate and coating, DSAs possess the unique properties of high electro-catalytic activity, long-term stability, low dissolution rate, high current efficiency, high anodic current density, low cell potential and excellent corrosion resistance in highly concentrated chloride solutions [3,5,8–11]. Recently, different attempts have been made to enhance the electro-catalytic activity, electrical conductivity, and chemical stability of these electrodes. It has been well documented that the coating composition is a major factor in controlling the electro-catalytic properties of the DSAs [12].

There are coatings which have high electro-catalytic activity and chemical stability; as well, they are affordable; the noble metal oxides such as IrO_2 and RuO_2, or other compounds like TiO_2, Ta_2O_5, ZrO_2, Co_3O_4, SiO_2, Nb_2O_5 and CeO_2 belong to this group. Accordingly, different types of these coatings, such as RuO_2–Ta_2O_5, IrO_2–TiO_2, IrO_2–Ta_2O_5, IrO_2–Nb_2O_5 and IrO_2–ZrO_2, have been developed for DSAs since the last decades [1,7,13–16].

Shao et al. [15] developed the IrO_2–ZrO_2 double component coatings prepared by the thermal decomposition method on titanium electrodes and observed that the electrode with 70 mol% IrO_2 showed the largest charge/discharge efficiency [15].

In another attempt, it has been reported that the presence of RhO_x can accelerate the hydrogenation of the unsaturated organic molecules and the dissociation of the nitrogen oxide. The coating of RhO_x on Ti substrate was found to be beneficial for O_2 evolution in acid solution [17]. Swette et al. [18] reported that the electrodes coated with of RhO_2 are highly stable against oxygen evolution and reduction. Compared to the RuO_2 and IrO_2, the coatings containing RhO_2 showed more increase in hydrogen evolution activity in acidic solutions [18].

However, Hrussanova et al. [19] stated that the electro-catalytic activity of RhO_x in the oxygen evolution was similar to IrO_2 in the 0.5 mol L^{-1} sulfuric acid solution, but RuO_2 showed more activity in the same solution [19]. As a matter of fact, combination of two or more oxides would change the electro-catalytic activity of DSAs due to the changes in the morphologies and the surface chemical composition [3,17].

* Corresponding author. Tel: +983133915735; fax: +98 313 3912752.
E-mail address: m.atapour@cc.iut.ac.ir (M. Atapour).

https://doi.org/10.1016/j.electacta.2019.135158
0013-4686/

In recent years, ternary and multiple oxides have also been introduced as other strategy to improve the stability and electrochemical activity of DSAs. Several investigations have been reported on oxide mixtures and their effects on the electrode performance. For example, Liu et al. [20] prepared RuO_2-doped Ti/IrO_2–ZrO_2 anodes and observed that the electrocatalytic activity was improved by increasing Ru content. Qin et al. [21] demonstrated that ternary IrO_2–SnO_2–Sb_2O_5 anodes with large mean curvature tend to increase the stability and durability for O_2 evolution even at 70 °C.

In this study, an effort was made to produce coatings with the composition of 70%IrO_2– 30%ZrO_2 by means of thermal decomposition. The use of electrodes consisting of IrO_2–ZrO_2 coatings has been studied previously [15] and it was found that this system is a promising candidate for electrochemical supercapacitors. However, IrO_2 is much expensive and its activity is not high [21]. To save cost and enhance the coating performance, the iridium oxide was substituted by different mole percent of Rhodium oxide to produce a triple component coating of IrO_2–RhO_x-ZrO_2 on the titanium substrates. In addition, ZrO_2 has a high corrosion resistance as well as excellent thermal stability, and has been used in a variety of applications such as fuel cells [15].

To the best of our knowledge, no studies have been conducted on the influence of the RhO_x amount on the electrochemical performance of IrO_2–ZrO_2 coating system. The aims of this work are therefore to study the microstructure and electrochemical characterization of IrO_2+RhO_x + ZrO_2 coated titanium anodes. X-ray diffraction, scanning electron microscopy, chrono-potentiometry (the potential versus time in constant current density), electrochemical impedance spectroscopy and cyclic voltammetry tests were used to study the effect of the changes in the chemical composition of the coatings on the structure, morphologies, chemical activity, electrical conductivity, coatings capacitance, electrochemically active surface areas and the coatings corrosion resistance.

2. Experimental

2.1. Materials preparation

The substrate for all coatings consisted of the pure commercial TA2 class titanium sheets with 2 mm thickness. Correspondingly, the sheets were sand blasted and cut in rectangular shapes with 15 × 15 mm dimensions. The substrates were soaked for 4 min in a boiling 50 vol% HCl solution. This step helped to clean the surface from any residual corrosion products, oxide layers and solid particles. Furthermore, the substrates were ultrasonically degreased in acetone for 15 min. Additionally, the substrates were acid washed for 2 h in the 10% boiling oxalic acid solution in order to obtain gray surfaces with the uniform roughness. Finally, the treated substrates were washed using double distilled water and kept under acetone.

Different metallic precursors like $IrCl_3.xH_2O$, $ZrOCl_2 \cdot 8H_2O$ and $RhCl_3 \cdot 3H_2O$ were individually dissolved in double distilled water for 2 h (the metallic cations concentration was 0.02 M) and then mixed together with different mole ratios. The traditional thermal decomposition method was used to make the precipitation of the mixed metal oxides on the substrate surface. First, the substrates were immersed in the solutions for 5 min and then brought out of the solution with the rate of 80 mm/min. However, the coated specimens were kept in the oven under 100 °C for 15 min in order to ensure the evaporation of the solvents.

Subsequently, the specimens were sintered in an air circulation furnace for 15 min and at 450 °C in order to form metal oxides on the surface. However, the last sequences were repeated 7 times to reach the adequate coating thickness. Finally, the specimens were heated in an air circulation furnace with the slow heating rate of 1 °C/min up to 550 °C; the temperature remained steady at 550 °C for 2 h. Then, the specimens were kept in the furnace to be cooled down; this was done to complete the final annealing procedure.

2.2. Materials characterization

2.2.1. Microstructure and chemical composition analysis

In order to verify the microstructure, surface morphology and elemental analysis of the coated electrodes, the Philips XL30 scanning electron microscope was used. Also, X-ray diffraction (XRD) patterns were used to evaluate and detect the oxide phases formed on the surface of the coated electrodes.

2.2.2. Electrochemical measurements

The electrochemical characterization of the thermally decomposed electrodes was performed using the accelerated life test (ALT), electrochemical impedance spectroscopy (EIS), and cyclic voltammetry (CV). All of the electrochemical tests were carried out in the 0.5 mol L^{-1} H_2SO_4 solution in a three-electrode corrosion cell with platinum as the counter electrode, saturated calomel electrode (SCE) as the reference electrode, and each specimen as the working electrode. All the tests were done using a potentio-stat, PAR 2273 model, after the OCP test for 3600 s. The CV curves were recorded in a range between 0.16 and 1.16 $V_{vs\ SCE}$ at the scanning rate of 20 mV s^{-1}. Cyclic Voltammetry test was also carried out during and after ALT in a range of 0.16–1.16 $V_{vs\ SCE}$ and the scanning rate of 20 mV s^{-1}. The EIS measurement was taken at the potential of 1.35 $V_{vs\ SCE}$, the frequency range of 10 mHz–100 kHz, and the potential amplitude of 5 mV at 41 points. Also, the EIS test was taken during and after ALT at 1.35 V. The impedance data were fitted to the appropriate equivalent electric circuit using the Z-view software. ALT was carried out under electrolysis at a constant current density of j = 2 A cm^{-2} in the 0.5 mol L^{-1} H_2SO_4 solution.

3. Results and discussion

3.1. Morphology characterization

The SEM micrographs of the IrO_2-RhO_x-ZrO_2 coated Ti electrodes are presented in Fig. 1. Fig. 1a shows a cracked muddy structure with some smooth areas (needle-like crystals) in the case of 70%IrO_2+30%ZrO_2 coating before the final annealing treatment. Some agglomerated small particles are also distinct in the cracked area. The formation of cracks, which is very classical for DSA electrodes, can be attributed to the difference between thermal expansion coefficients of the titanium substrate and the coating components. Also, the solvent volatilization and generation of thermal stresses during continuous heating and cooling cycles are other sources of cracking [22].

In fact, one of the disadvantages of 70%IrO_2+30%ZrO_2 coatings may be the existence of such cracks, providing the routes for oxygen and electrolyte and allowing the substrate to be oxidized faster. However, the existence of these cracks could increase the effective surface of the electrode, which would have a relatively positive effect on its electro-catalytic behavior. It has been reported that these cracked morphologies could cause chlorine and oxygen to be released more easily [3,15]. As shown in Fig. 1b, the cracks were covered by glowing prismatic columnar crystals (with the diameter of 40–80 nm) after final annealing at 550 °C for 2 h. The mentioned crystalline particles could increase the electrical conductivity of the electrode. It has been reported that the critical crystallization temperature of the Ti/IrO_2–ZrO_2 electrodes was in the range of 340–360 °C [15]. The changes in the oxide coating morphology showed the higher crystallization degree in the final annealing step at 550 °C, in comparison to the sintering at 450 °C.

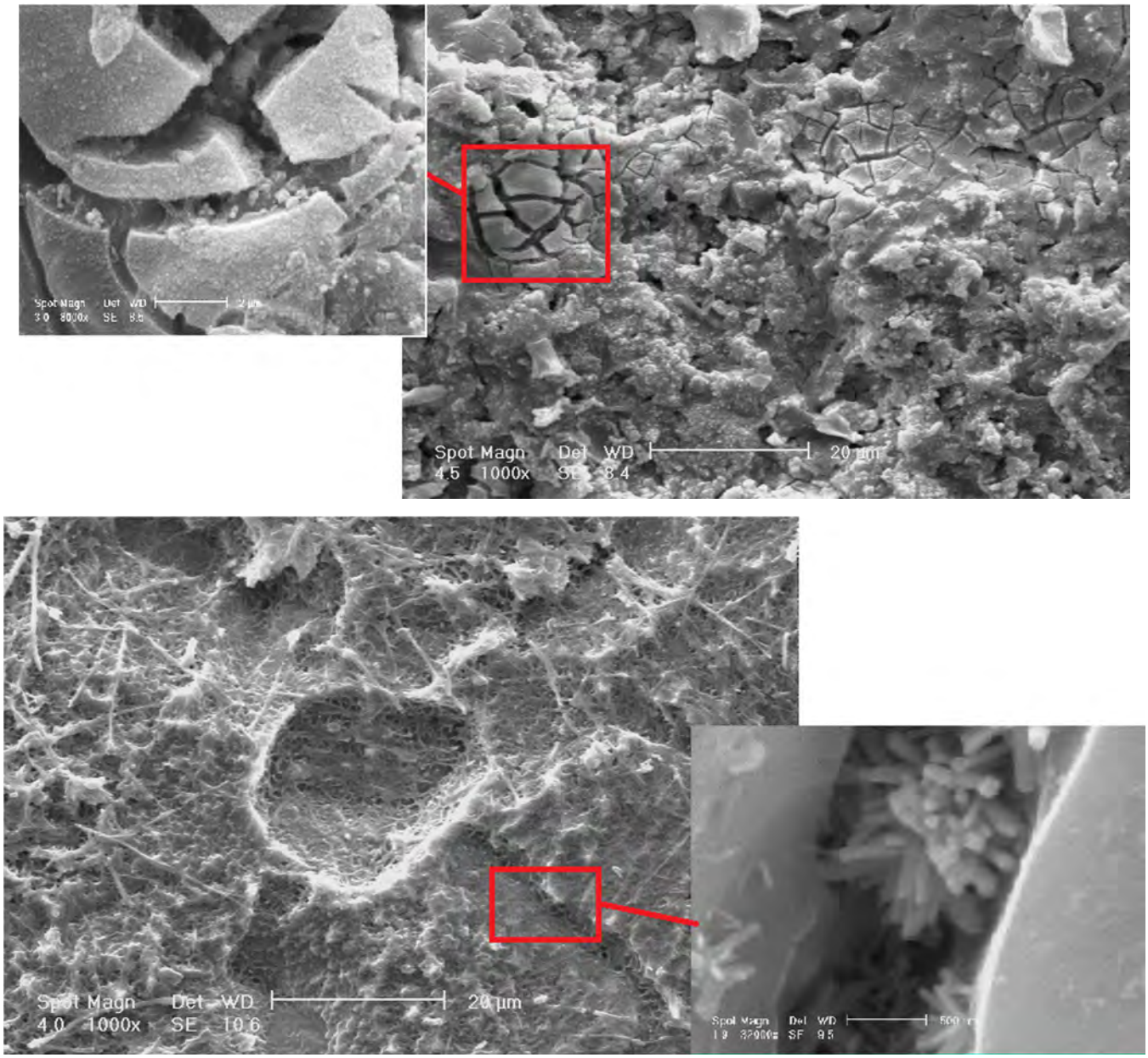

Fig. 1. SEM micrographs of Ti/70%IrO_2–30%ZrO_2: a. before final annealing, and b. after final annealing.

The surface morphology of different IrO_2+RhO_x + ZrO_2 coatings are presented in Fig. 2. These coatings reveal a typical porous "cracked mud" morphology. Some oxide particles were deposited inside the cracks. Also, it can be seen that the increase in the mole percentage of RhO_x accelerated the formation of cracks. This phenomenon [23] can be explained by the low interaction of the TiO_2, IrO_2 and RhO_2 tetragonal structures with the rhombohedral Rh_2O_3. Accordingly, different crystallographic structures of coating components could be responsible for the formation of non-compact coatings with a high porosity/roughness degree that accelerating the formation of the passive layer [23,24]. Fig. 2e shows the formation of some wide and deep cracks with cellular morphology in the case of 10%IrO_2+60%RhO_x+30%ZrO_2.

3.2. XRD analysis

The X-ray diffraction patterns of different mixed metal oxide anodes are shown in Fig. 3. The XRD pattern of the 70%IrO_2+30% ZrO_2 coating revealed the characteristic peaks of IrO_2 and the sharp peaks of Ti substrate. The related 2Θ/degrees of the IrO_2 tetragonal phase peaks were 27.8492, 34.5654 and 53.7753, which were shifted to the lower degrees in comparison to the standard peaks. The standard 2Θ values for the mentioned peaks are 28.055, 34.715 and 54.025. The mentioned phenomenon showed the increase of the mean space of the crystalline lattice of IrO_2. Based on crystallinity considerations, it seems the increase in lattice volume is due to some substitution of Ir^{4+} ions with 0.0625 nm radius by Zr^{4+} ions with 0.072 nm radius. These results can be an important evidence on the formation of IrO_2–ZrO_2 solid solution. Also, these interstitial defects can lead to the lattice distortions [15].

The XRD patterns of Ti/IrO_2-RhO_x-ZrO_2 anodes contained Ti, RhO_x and IrO_2 peaks. The Ti peaks came from the substrate. The presence of RhO_2 and IrO_2 tetragonal phases confirmed that there was a RhO_2–IrO_2 solid solution in the surface coating. It should be

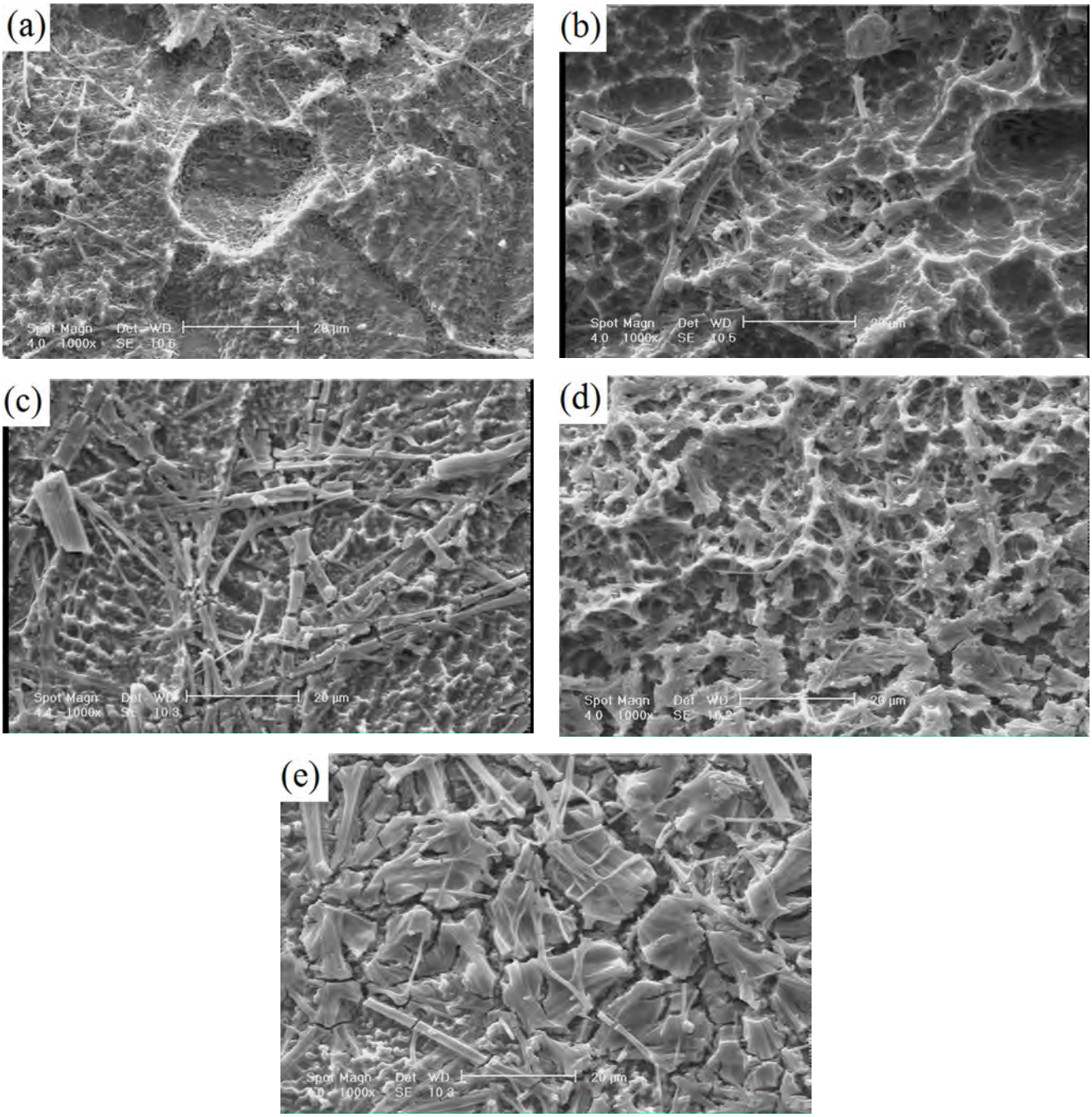

Fig. 2. SEM micrographs of the coated anodes: a. Ti/70%IrO_2−30%ZrO_2, b. Ti/55%IrO_2-15%RhO_x-30%ZrO_2, c. Ti/40%IrO_2-30%RhO_x-30%ZrO_2, d. Ti/25%IrO_2-45%RhO_x-30%ZrO_2, and e. Ti/10%IrO_2-60%RhO_x-30%ZrO_2.

noted that rhodium ions have two forms of Rh^{4+} in the tetragonal phase of RhO_2 and Rh^{3+} in the rhombohedral phase of Rh_2O_3 [17]. It seems some small amounts of RhO_2 transformed to the Rh_2O_3 rhombohedral phases. It is due to the high calcination temperature (higher than 500 °C).

3.3. Accelerated life test (ALT)

The stability of the IrO_2+RhO_x + ZrO_2 anodes was examined by accelerated life test (ALT) carried out at high current density ($j = 2\,A\,cm^{-2}$). As shown in Fig. 4, all electrodes exhibit a similar curve consisting of three different stages of activating, stability and deactivation. Similar trends have previously been reported for the majority of MMO anodes [10]. The small drop in the first step of exposure can be related to the penetration of the electrolyte into the inner surfaces like cracks, porosities and grain boundaries. As mentioned before, these defects were formed during the thermal decomposition process and provided some active surface points for OER during the electrolysis. After a small drop, the potential was increased and then remained relatively constant in steady state condition. The rising of the potentials can be due to the removal of non-adherent oxides (elimination of the active layer's outer pores)

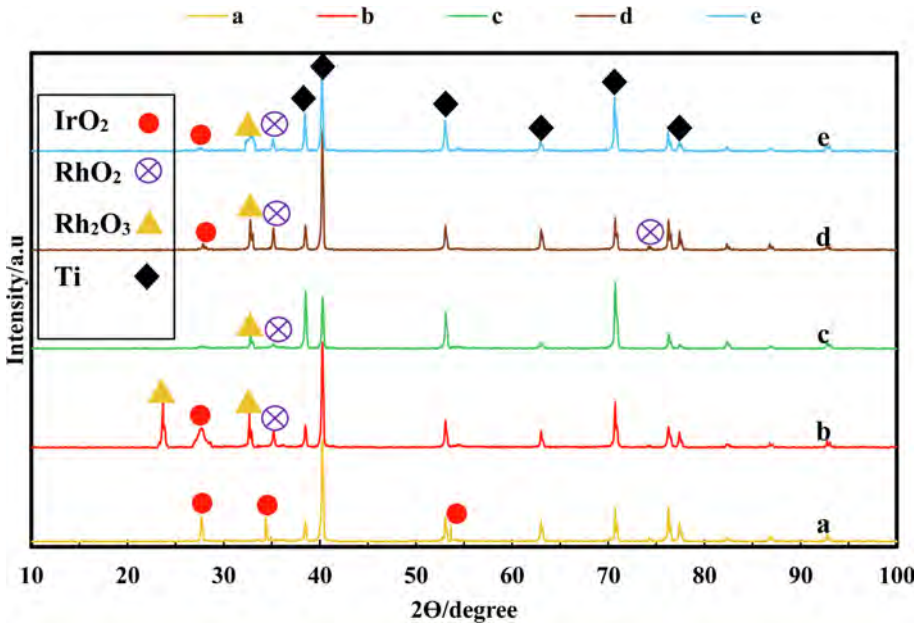

Fig. 3. X-ray diffraction patterns of a. Ti/70%IrO_2−30%ZrO_2, b. Ti/55%IrO_2-15%RhO_x-30%ZrO_2, c. Ti/40%IrO_2-30%RhO_x-30%ZrO_2, d. Ti/25%IrO_2-45%RhO_x-30%ZrO_2, and e. Ti/10%IrO_2-60%RhO_x-30%ZrO_2.

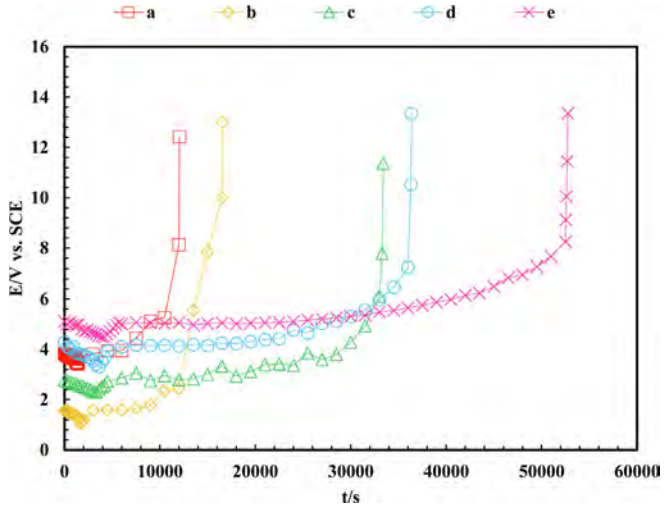

Fig. 4. Chrono-potentiometry curves of a. Ti/70%IrO_2−30%ZrO_2, b. Ti/55%IrO_2-15%RhO_x-30%ZrO_2, c. Ti/40%IrO_2-30%RhO_x-30%ZrO_2, d. Ti/25%IrO_2-45%RhO_x-30%ZrO_2, and e. Ti/10%IrO_2-60%RhO_x-30%ZrO_2 in the 0.5 mol L^{-1} H_2SO_4 at j = 2 A cm^{-2}.

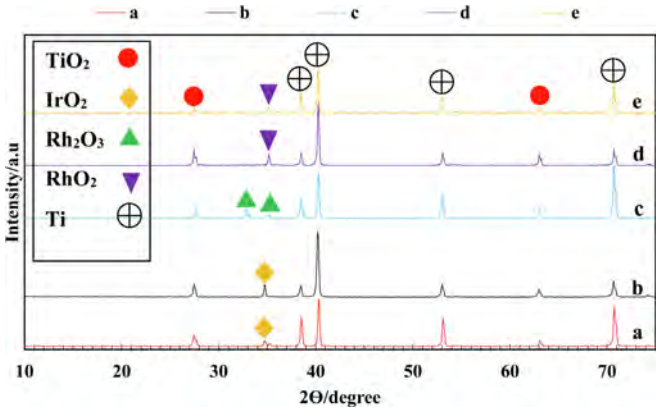

Fig. 5. X-ray diffraction patterns of a. Ti/70%IrO_2−30%ZrO_2, b. Ti/55%IrO_2-15%RhO_x-30%ZrO_2, c. Ti/40%IrO_2-30%RhO_x-30%ZrO_2, d. Ti/25%IrO_2-45%RhO_x-30%ZrO_2, and e. Ti/10%IrO_2-60%RhO_x-30%ZrO_2 after ALT.

by corrosion and erosion. Finally, the elimination of the electrocatalytic layer and the anodic growth of TiO_2 middle layer would cause a sharp increase in the potential and initiation of the deactive region [3,9,10].

According to the Fig. 4, the accelerated service time for the specimen with 60%RhO_x (10%IrO_2+60%RhO_x+30%ZrO_2) was the highest (52500 s), while that for the coating without RhO_x was the lowest (12000 s). In other words, the anode service time was enhanced by increasing the concentration of RhO_x in coatings. Some researches [5,9] stated that the addition of IrO_2 increased the stability of the coatings. However, the formation of soluble species like IrO_4^{2-} at high potentials such as 2 V that occurred in this work leads to the rapid destruction of the coating [25]. According to the results of ATL evaluations, the addition of RhO_x promoted the service life of anodes because of the lower dissolution rate of the catalytic layer. However, more systematic studies are needed to evaluate the electrochemical stability of Ti/70% RhO_x-30%ZrO_2 electrodes. In an attempt, Swette et al. [18] evaluated the electrochemical stability of the RhO_2 electrodes and reported that these types of electrodes are very stable in terms of oxygen evolution and reduction. Roginskaya et al. [26] studied the electrochemical properties of Ti/RhO_x electrodes made by thermal decomposition method. Their results clarified that rhodium oxide (RhO_x) is much more stable than RuO_2 and IrO_2 in acidic solutions. Hrussanova et al. [19] focused on the electrochemical behavior of RhO_x electrodes based on the oxygen evolution in acidic solutions. They reported that the oxygen evolution was not able to degrade the RhO_x electrodes after the initial removal of loose particles. Therefore, it can be deduced that the RhO_x coatings are able to show high stability. Also, the Ti/70%RhO_x-30%ZrO_2 electrode is expected to have the higher stability than the Ti/70%IrO_2−30%ZrO_2 electrode.

After the end of the electrolysis time, the amounts of voltammetry anodic charge for all electrodes were in the range of 12−25%

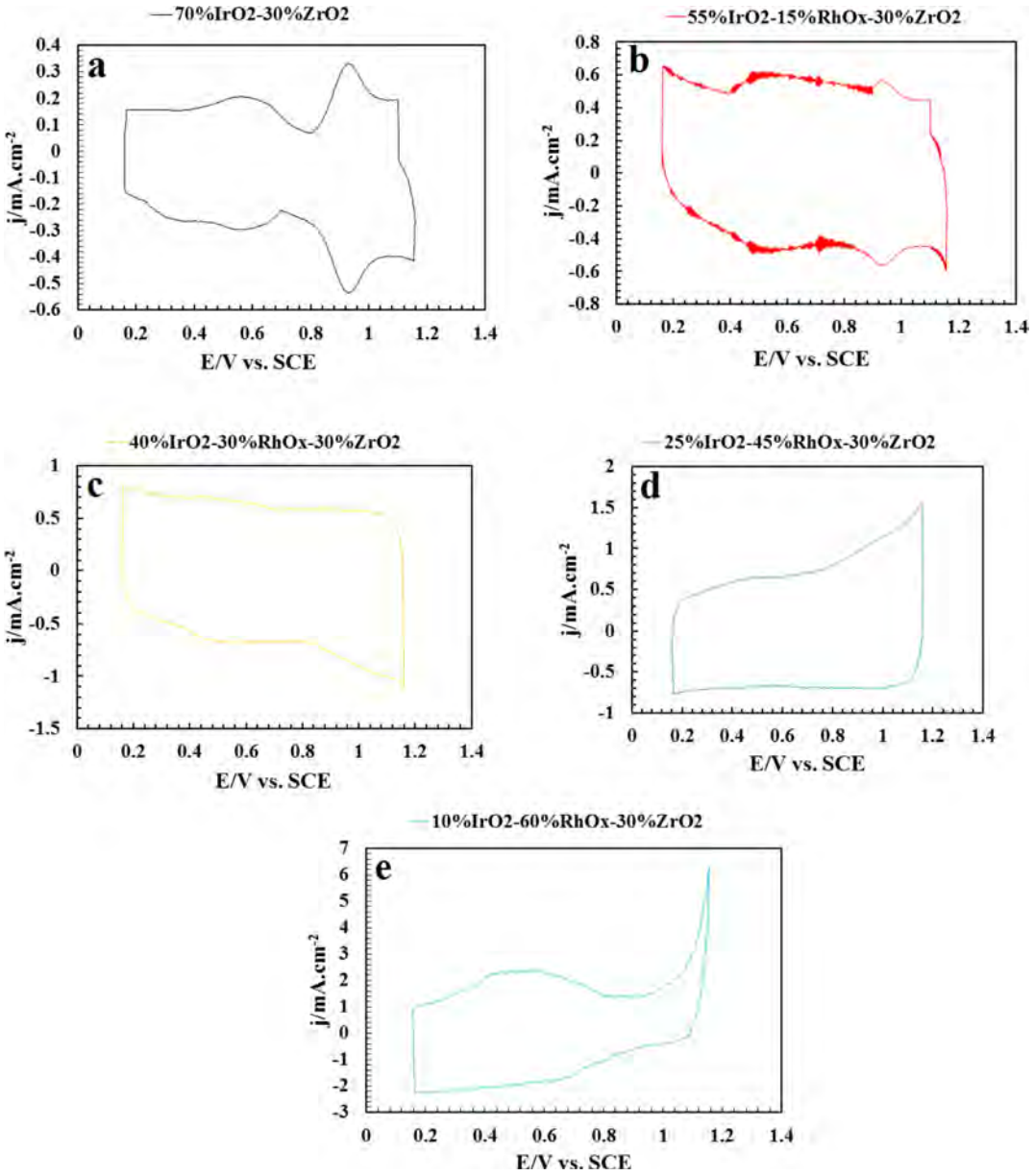

Fig. 6. Cyclic voltammetry curves of a. Ti/70%IrO_2−30%ZrO_2, b. Ti/55%IrO_2-15%RhO_x-30%ZrO_2, c. Ti/40%IrO_2-30%RhO_x-30%ZrO_2, d. Ti/25%IrO_2-45%RhO_x-30%ZrO_2, and e. Ti/10%IrO_2-60%RhO_x-30%ZrO_2 as a function of chemical composition in the 0.5 mol L^{-1} H_2SO_4 at the scanning rate of 20 mV/s.

Table 1
Two pairs of the redox transition peaks values for the all coatings.

Specimen	First pairs of redox transition peaks/V	Second pairs of redox transition peaks/V
70%IrO_2−30%ZrO_2	0.4−0.7	0.84−1.04
55%IrO_2-15%RhO_x-30%ZrO_2	0.4−0.76	0.84−1.04
40%IrO_2-30%RhO_x-30%ZrO_2	0.4−0.8	–
25%IrO_2-45%RhO_x-30%ZrO_2	0.44−0.64	–
10%IrO_2-60%RhO_x-30%ZrO_2	0.6−0.92	0.96−1.08

of the initial values. Moreover, an increase of the anodic potential in the de-active region can be related to the destruction of the oxide layer and the formation of a non-conductor TiO_2 layer (with rutile structure) in the Ti/oxide layer interfaces. This was confirmed according to the presence of some sharp peaks for TiO_2 in the XRD patterns (Fig. 5). Also, the physical impedances relating to the inner surface of oxide layer and the Ti/oxide interface were also sharply increased similar to other investigations [10,27].

3.4. Cyclic voltammetry

Fig. 6 shows the cyclic voltammetry diagrams of different anodes in 0.5 mol L^{-1} H_2SO_4 solution at a sweep rate of 20 mV/s and the potential range of 0.16−1.16 $V_{vs\ SCE}$. The selected potential range

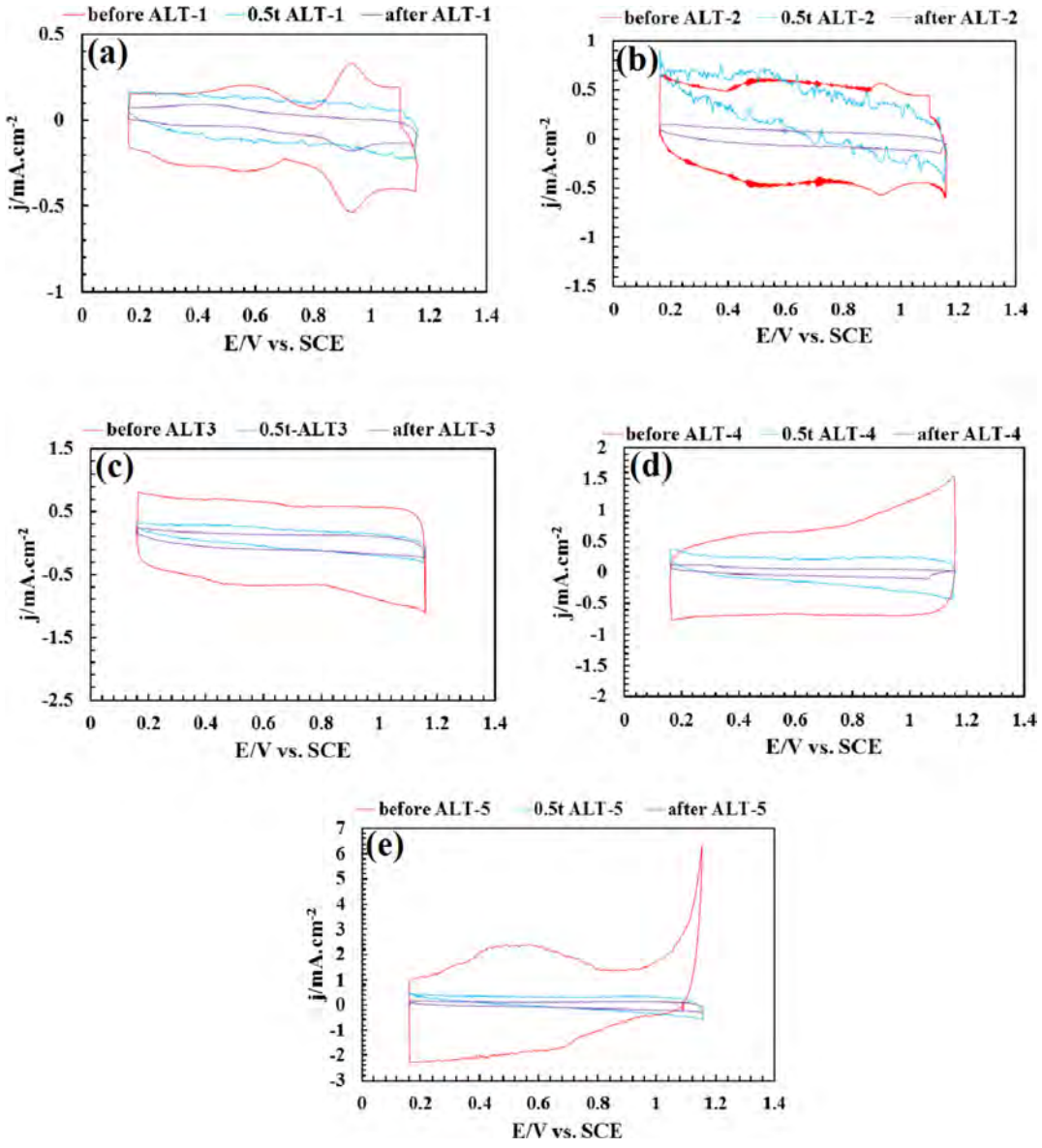

Fig. 7. Cyclic voltammetry curves of a. Ti/70%IrO_2−30%ZrO_2, b. Ti/55%IrO_2-15%RhO_x-30%ZrO_2, c. Ti/40%IrO_2-30%RhO_x-30%ZrO_2, d. Ti/25%IrO_2-45%RhO_x-30%ZrO_2, and e. Ti/10%IrO_2-60%RhO_x-30%ZrO_2 as a function of the electrolysis time in the 0.5 mol L^{-1} H_2SO_4 at the scanning rate of 20 mV/s.

Table 2
q* values vs electrolysis time for the all coatings, with the scanning rate of 20 mV/s in the 0.5 mol L^{-1} H_2SO_4 solution (t_{6v} is the electrode service life).

Specimen	q^*_a/mC.cm^{-2} ($t_1 = 0$)	q^*_a/mC.cm^{-2} ($t_2 = 0.5\ t_{6v}$)	q^*_a/mC.cm^{-2} ($t_3 = t_{6v}$)
70%IrO_2−30%ZrO_2	23.49	11.63	5.94
55%IrO_2-15%RhO_x-30%ZrO_2	46.13	20.44	6.89
40%IrO_2-30%RhO_x-30%ZrO_2	65.15	13.69	11.37
25%IrO_2-45%RhO_x-30%ZrO_2	72.46	20.00	5.25
10%IrO_2-60%RhO_x-30%ZrO_2	104.12	20.09	10.72

was between the hydrogen and oxygen evolution ranges. Voltammetry charge could be used to estimate the electrochemically active surface regions [8]. Fig. 6 represents the effect of the increasing the Rh content in the surface coating of the MMO anodes. Based on Fig. 6, all coatings exhibited approximately similar curves with two peaks of redox at the potential range of 0.4−0.8 V and 0.84−1.12 V. These peaks show the presence of the solid-state redox transitions Ir(III)/Ir(IV) and Ir(IV)/Ir(V) [6]. Two pairs of the redox transition peak values for the all specimens are shown in Table 1.

According to the anodic-cathodic symmetry observed in Fig. 6, it can be concluded that the redox sites were reversible and exhibited a quasi-capacitor behavior. Moreover, it has been reported that the MMO anodes preserve their initial surface conditions in terms of species absorption and valence variation due to the occurrence of reversible redox reactions [3,28]. The observation of two pairs of broad cathodic and anodic peaks in the CV plot of 10%IrO_2+60% RhO_x+30% ZrO_2 anode can be due to the heterogeneity of the active sites on the surface of coating [29]. It seems the peaks associated

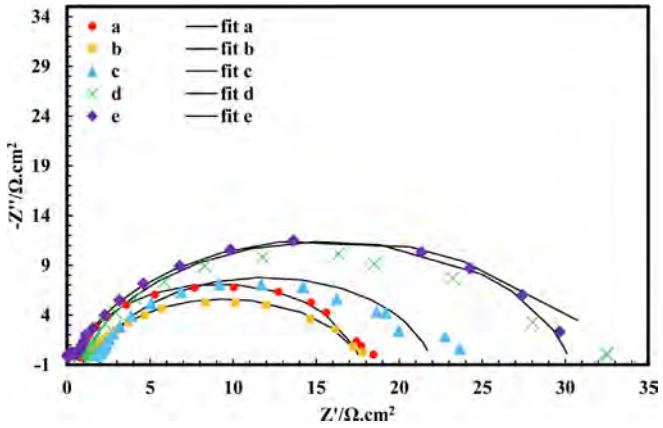

Fig. 8. Nyquist diagrams of a. Ti/70%IrO_2—30%ZrO_2, b. Ti/55%IrO_2-15%RhO_x-30%ZrO_2, c. Ti/40%IrO_2-30%RhO_x-30%ZrO_2, d. Ti/25%IrO_2-45%RhO_x-30%ZrO_2, and e. Ti/10%IrO_2-60%RhO_x-30%ZrO_2 in the 0.5 mol L^{-1} H_2SO_4 at the potential of 1.35 V_{SCE}, (geometric shapes) the experimental data, and the (−) fitted data.

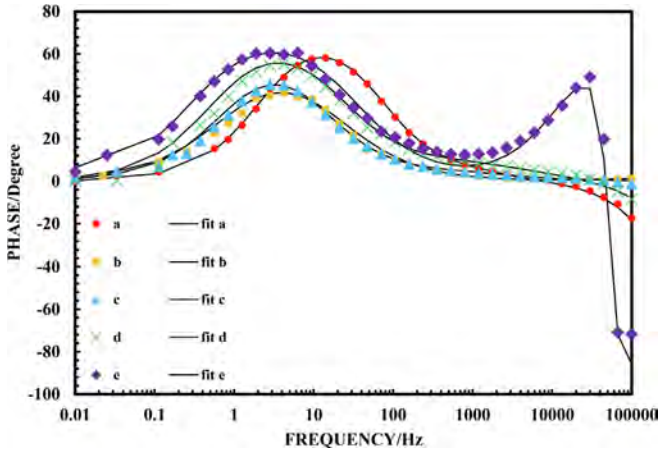

Fig. 9. Bode-phase plots of a. Ti/70%IrO_2—30%ZrO_2, b. Ti/55%IrO_2-15%RhO_x-30%ZrO_2, c. Ti/40%IrO_2-30%RhO_x-30%ZrO_2, d. Ti/25%IrO_2-45%RhO_x-30%ZrO_2, and e. Ti/10%IrO_2-60%RhO_x-30%ZrO_2 in the 0.5 mol L^{-1} H_2SO_4 at the potential of 1.35 V_{SCE}, (geometric shapes) the experimental data, and the (−) fitted data.

with redox reactions of Rh (III)/Rh (IV) were disappeared due to the presence of chloride in the oxide layer [30]. Similarly, it has been reported that for Ti anodes with the RhO_x coating made by H_3RhCl_6, the obvious band of redox transitions was not observed in their CV

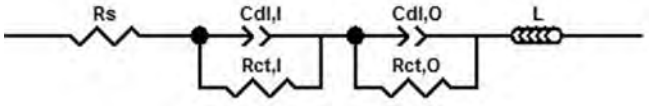

Fig. 10. The equivalent electrical circuit model used to simulate the impedance data.

Table 4
$C_{dl,I}$ and $C_{dl,O}$ values for all specimens were calculated using the equation (2) and the impedance parameters shown in Table 3 in a stable potential of 1.35 V $_{vs\ SCE}$.

Specimen	$C_{dl,I}$/mF.cm^{-2}	$C_{dl,O}$/mF.cm^{-2}	Chi-squared
70%IrO_2 + 30%ZrO_2	0.00007	3.07	3.3×10^{-3}
55%IrO_2 + 15%RhO_x + 30%ZrO_2	1.02	6.10	8.7×10^{-3}
40%IrO_2 + 30%RhO_x + 30%ZrO_2	0.75	6.44	5.1×10^{-3}
25%IrO_2 + 45%RhO_x + 30%ZrO_2	0.44	5.46	7.9×10^{-3}
10%IrO_2 + 60%RhO_x + 30%ZrO_2	0.02	5.25	1.5×10^{-2}

curves. The solid-state surface redox transitions exhibited a quasi-capacitor behavior associated with the transmission of protons. The most common proton exchange reaction is based on the Eq. (1) [3].

$$MO_x(OH)_y + \delta H^+ + \delta e^- = MO_{x-\delta}(OH)_{y+\delta} \quad (1)$$

The anodic voltammetry charge (q^*) was measured by graphical integration of the j-E curves. q^* specifies the amount of the exchanged proton and it is proportional to the number of surface active sites. Fig. 6 illustrates that q^* is dependent on the type of the chemical composition of the applied coating on the substrate. The surface active areas of the electrode were raised by increasing the RhO_x concentration due to the formation of more porosity and cracks in the morphology of the coatings. In other words, the q^* increased by improving the electro-catalyzer activity due to raising the active areas. Several authors [23] introduced a parameter to identify the degree of electrode instability from the E versus t-results. It is named as t_{6V} which provides the electrode service life. The overall outcome is that while the 70%IrO_2—30%ZrO_2 coating exhibited a good electrical conductivity, but it was not a good candidate for proton exchange. In order to achieve more details about the dynamics of the changes occurred on the coatings, the cyclic voltammetry tests were carried out on the specimens at different anodizing times, as shown in Fig. 7. It can be seen that the CV curves were changed in different times and the voltammetry j reduced with raising t. The q^*_a values for all specimens at different anodizing times were extracted and presented in Table 2.

Generally, it can be seen that for all coatings the q^*_a decreased with increasing t, in accordance with the results reported by Da Silva on the Ti/(Ru + Ti + Ce)O_2-system. Such behavior can be explained based on the following phenomena [9,23]:

1 The erosion of loose and non-adhesive oxide particles due to the aggressive gas evolution in the primary times.
2 The corrosion of oxides associated with the high over-potentials let to the creation of some soluble species.
3 The passivation of the Ti substrate due to the presence of a porous coating and the penetration of electrolyte into coating and its interactions with substrate.

3.5. Electrochemical impedance spectroscopy (EIS)

The EIS response of different IrO_2-RhO_x-ZrO_2 coated Ti anodes in H_2SO_4 solution was evaluated at an applied dc potential of 1.35 V

Table 3
The fitting EIS parameters of different specimens in 0.5 mol L^{-1} H_2SO_4, E_{appl} = 1.35 V $_{vs\ SCE}$.

Specimen	R_s/Ω.cm^2	Q_f/Ω^{-1}.cm^{-2}.s^n	n	$R_{ct,I}$/Ω.cm^2	Q_{dl}/Ω^{-1}.cm^{-2}.s^n	n	$R_{ct,O}$/Ω.cm^2	L/H.cm^2
70%IrO_2 + 30%ZrO_2	0.71	3.1×10^{-3}	0.70	0.05	5.6×10^{-3}	0.90	16.63	3.7×10^{-7}
55%IrO_2 + 15%RhO_x + 30%ZrO_2	1.48	1.0×10^{-2}	0.75	0.151	1.8×10^{-2}	0.78	16	–
40%IrO_2 + 30%RhO_x + 30%ZrO_2	1.68	1.0×10^{-2}	0.69	0.34	1.3×10^{-2}	0.85	19.79	–
25%IrO_2 + 45%RhO_x + 30%ZrO_2	0.74	1.5×10^{-2}	0.61	0.43	1.3×10^{-2}	0.85	28.94	2×10^{-7}
10%IrO_2 + 60%RhO_x + 30%ZrO_2	0.05	3.5×10^{-5}	0.95	0.56	2.1×10^{-2}	0.83	30.41	5.2×10^{-7}

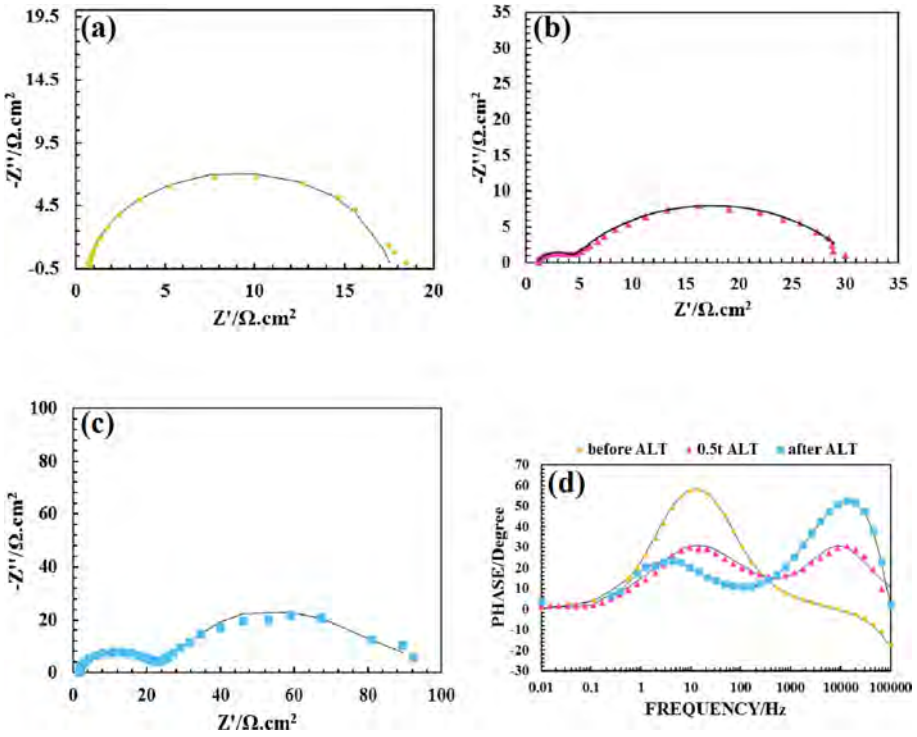

Fig. 11. (a), (b) and (c). Nyquist diagrams of Ti/70%IrO_2−30%ZrO_2 at, respectively, $t_1 = 0$, $t_2 = 0.5t_{6v}$ and $t_3 = t_{6v}$ in the 0.5 mol L^{-1} H_2SO_4 at the potential of 1.35 V_{SCE}, (d). Bode-phase plots of the specimen 1.

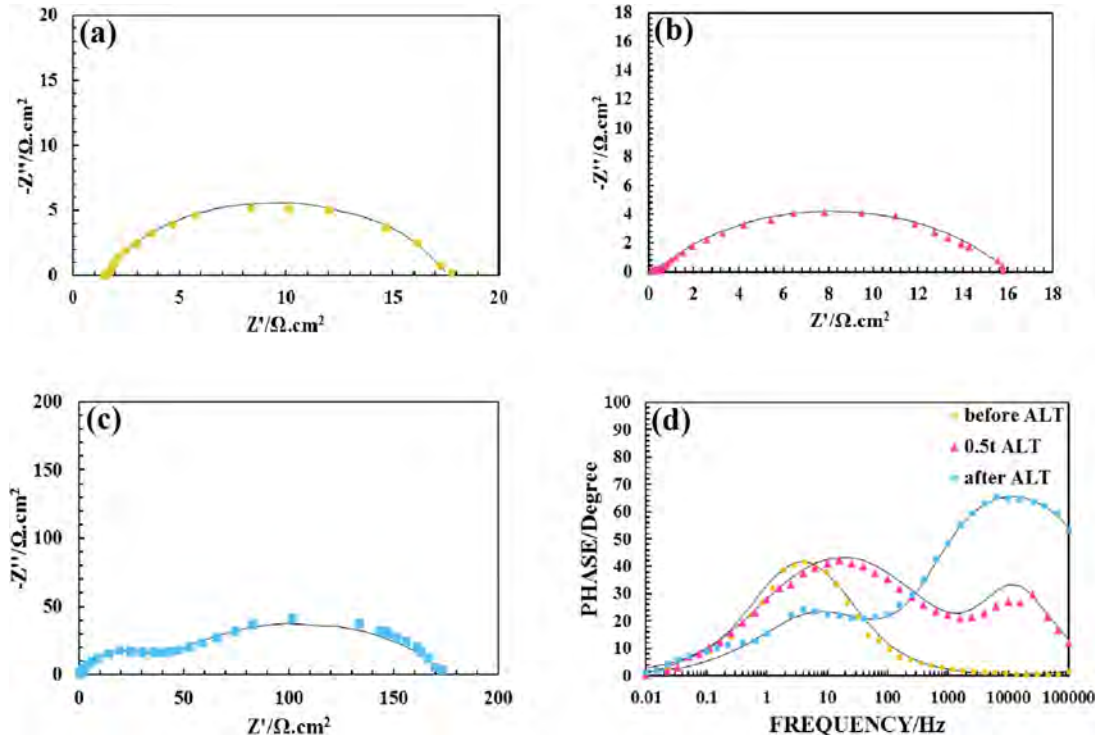

Fig. 12. (a), (b) and (c). Nyquist diagrams of the Ti/55%IrO_2-15%RhO_x-30%ZrO_2 at, respectively, $t_1 = 0$, $t_2 = 0.5t_{6v}$ and $t_3 = t_{6v}$ in the 0.5 mol L^{-1} H_2SO_4 at the potential of 1.35 V_{SCE}, (d). Bode-phase plots of the specimen 2.

(vs. SCE) and presented in Figs. 8 and 9. As shown in the Nyquist plots (Fig. 8), the impedance spectra of the coatings were similar in form, all consisted of a well-developed semi-circle at low and middle-frequency ranges and a small semi-circle at high-frequency ranges. The oxygen evolution reaction (OER) and the physical impedance covering the interface of the oxide layer/Ti substrate, were identified as the main phenomena in the low and high frequency domains, respectively [10]. The formation of the irregular

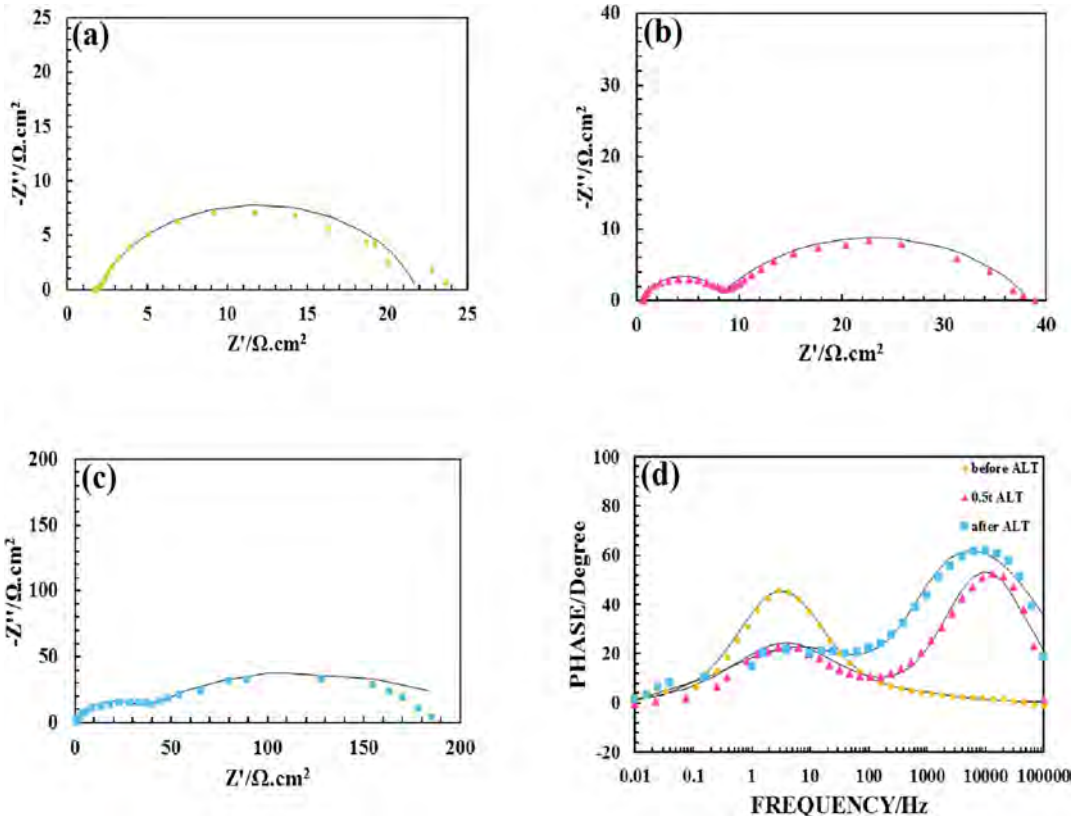

Fig. 13. (a), (b) and (c). Nyquist diagrams of the Ti/40%IrO_2-30%RhO_x-30%ZrO_2 at, respectively, $t_1 = 0$, $t_2 = 0.5t_{6v}$ and $t_3 = t_{6v}$ in the 0.5 mol L^{-1} H_2SO_4 at the potential of 1.35 V_{SCE}, (d). Bode-phase plots of the specimen 3.

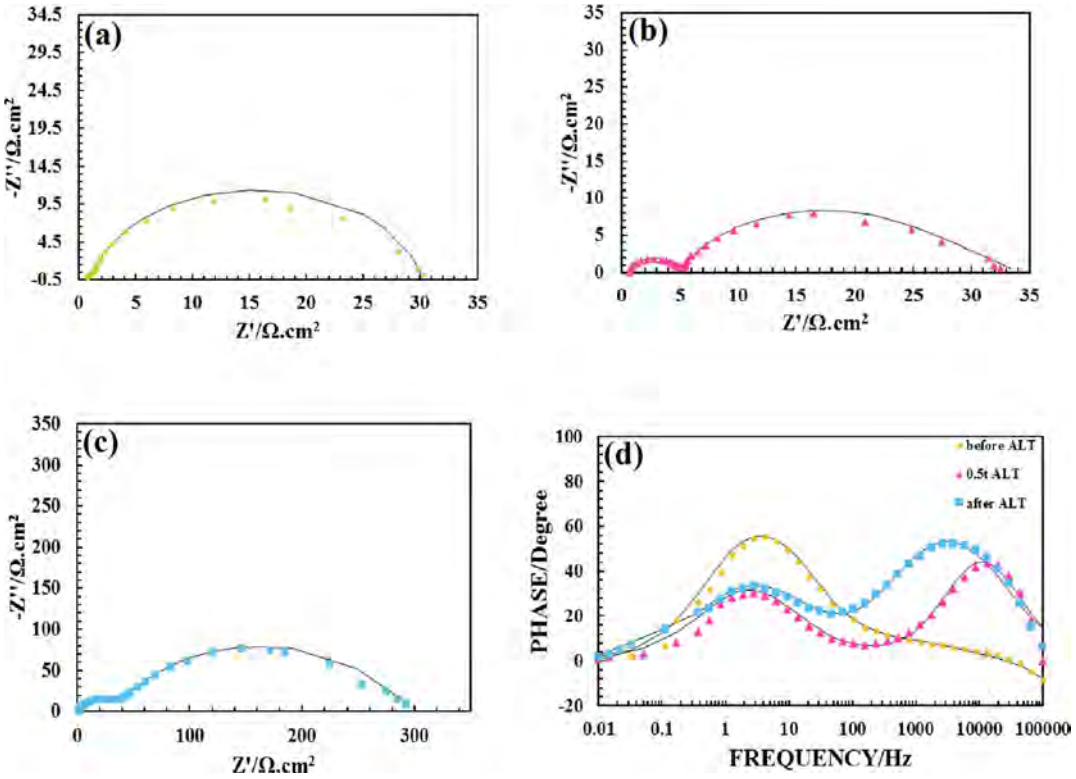

Fig. 14. (a), (b) and (c). Nyquist diagrams of Ti/25%IrO_2-45%RhO_x-30%ZrO_2 at, respectively, $t_1 = 0$, $t_2 = 0.5t_{6v}$ and $t_3 = t_{6v}$ in the 0.5 mol L^{-1} H_2SO_4 at the potential of 1.35 V_{SCE}, (d). Bode-phase plots of the specimen 4.

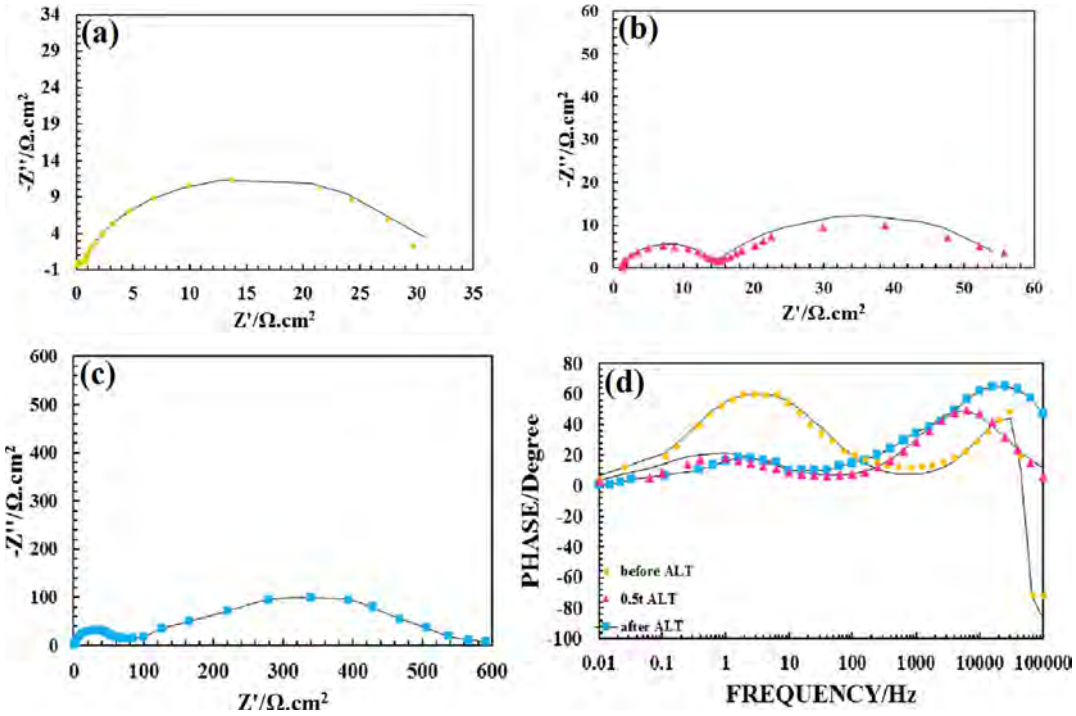

Fig. 15. (a), (b) and (c). Nyquist diagrams of the Ti/10%IrO_2-60%RhO_x-30%ZrO_2 at, respectively, $t_1 = 0$, $t_2 = 0.5t_{6v}$ and $t_3 = t_{6v}$ in the 0.5 mol L^{-1} H_2SO_4 at the potential of 1.35 V_{SCE}, (d). Bode-phase plots of the specimen 5.

semicircles can be related to the resistance of TiO_2 film and OER in the internal regions of the coatings [23]. Da Silva et al. [23] reported that the impedance at high frequencies can be affected by the crystallinity of the oxide layer and the level of doping of the TiO_2 by other coating components. It seems the physical characteristics of the porous structure of coatings are important because the center of the high-frequency arc was not located on the real axis [5]. Furthermore, the presence of inductance (L) was probably due to the porous nature of the coating produced by the thermal decomposition method [5,23]. Da Silva et al. [31] have recently suggested that the main reason for the inductive behavior can be the irregular charge transfer through the complex microstructure of the oxide layers. The equivalent electrical circuit model used to simulate the impedance data was R_s ($R_{ct,I}$, $C_{dl,I}$) ($R_{ct,O}$, $C_{dl,O}$) L (Fig. 10). The fitting parameters were extracted and shown in Table 3, where R_s, $R_{ct,I}$ and $R_{ct,O}$ represent the solution resistance, charge transfer resistance at the internal active surface and the charge transfer resistance at the external active surface, respectively. $C_{dl,I}$ is the double-layer capacity at the interface between the internal surface/electrolyte and $C_{dl,O}$ is the double-layer capacity at the interface between the outer surface/solution. The ideal capacitors were replaced by the constant phase elements (Q_{dl} and Q_f) because of the porous and cracked nature of the coatings.

The EIS results of the coatings presented in Table 3 demonstrated that the charge transfer resistance at the external active surface increased with addition of RhO_x content. It can be also deduced that the addition of RhO_x decreased the electro catalytic activity for oxygen evolution on the coated electrodes. The coating without RhO_x exhibited the lowest $R_{ct,O}$. Also, it was found that the electrical conductivity of coatings was decreased by increasing the rhodium oxide.

According to the literature [15], the degree of crystallinity is also

Table 5
Impedance parameters for all specimens at different electrolysis times extracted from fitting the experimental data to the equivalent electrical circuit in 0.5 mol L^{-1} H_2SO_4, $E_{appl} = 1.35$ $V_{vs\ SCE}$.

Specimen	t/s	$R_s/\Omega.cm^2$	$Q_f/\Omega^{-1}.cm^{-2}.s^n$	n	$R_{ct,I}/\Omega.cm^2$	$Q_{dl}/\Omega^{-1}.cm^{-2}.s^n$	n	$R_{ct,O}/\Omega.cm^2$	$L/H.cm^2$
70%IrO_2 + 30%ZrO_2	0	0.71	3.1×10^{-3}	0.70	0.05	5.6×10^{-3}	0.90	16.63	3.7×10^{-7}
	6000	1.08	6.0×10^{-5}	0.84	3.17	4.7×10^{-3}	0.69	26.52	–
	12000	1.55	7.0×10^{-6}	0.92	18.92	3.3×10^{-3}	0.67	76.02	–
55%IrO_2 + 15%RhO_x + 30%ZrO_2	0	1.47	9.6×10^{-3}	0.75	0.15	1.8×10^{-2}	0.78	16	–
	8250	0.11	2.1×10^{-4}	0.92	0.26	2.1×10^{-2}	0.63	16.61	–
	16500	0.22	2.8×10^{-5}	0.84	36.03	1.5×10^{-3}	0.63	138.5	–
40%IrO_2 + 30%RhO_x + 30%ZrO_2	0	1.68	1.0×10^{-2}	0.69	0.34	1.3×10^{-2}	0.85	19.79	–
	16500	0.60	1.9×10^{-5}	0.92	7.25	9.0×10^{-3}	0.66	30.66	–
	33000	0.53	2.2×10^{-5}	0.88	30.89	2.2×10^{-3}	0.57	156.9	–
25%IrO_2 + 45%RhO_x + 30%ZrO_2	0	0.75	1.5×10^{-2}	0.61	0.43	1.3×10^{-2}	0.85	28.94	1.9×10^{-7}
	18000	0.71	1.8×10^{-5}	0.94	4.16	1.3×10^{-2}	0.75	28.452	–
	36000	1.48	1.8×10^{-5}	0.82	32.19	1.5×10^{-3}	0.70	260.5	–
10%IrO_2 + 60%RhO_x + 30%ZrO_2	0	0.06	3.5×10^{-5}	0.95	0.56	2.1×10^{-2}	0.83	30.41	5.2×10^{-7}
	26250	1.23	2.6×10^{-5}	0.89	13.30	1.6×10^{-2}	0.69	37.96	–
	52500	1.02	1.2×10^{-5}	0.91	60.27	1.4×10^{-3}	0.69	520.85	–

a key factor influencing the electrochemical parameters. The crystallinity critical temperature (T_c) of the binary coatings with the Ir/Zr = 7/3 M ratio is reported to be in the range of 340–360 °C [15]. T_c of the coating films containing RhO_x was about 500 °C [29]. The sintering temperature of the anodes was 450 °C and the final annealing temperature was about 550 °C and these temperatures were much higher than the $T_{c,}$ of the binary coatings. Thus, it is expected that the IrO_2–ZrO_2 coated anodes exhibit very high degree of crystallinity and high electrical conductivity. 550 °C was slightly higher than the crystallinity, $T_{c,}$ of the films containing RhO_x. Therefore, it can be concluded that the presence of a mixture of crystalline and amorphous phases let to the increase of $R_{ct,I}$. The capacitances ($C_{dl,O}$ and $C_{dl,I}$) of the double layer was calculated according to the Equation (2) and shown in the Table 4 [6]:

$$C_{dl} = (Y_0)^{\frac{1}{n}} \cdot \left(\frac{1}{R_s} + \frac{1}{R_{ct}}\right)^{\frac{(n-1)}{n}} \quad (2)$$

At the applied potential of 1.35 V, the lowest $C_{dl,O}$ values were obtained for the IrO_2–ZrO_2 coated anode and the highest $C_{dl,O}$ values was related to the ternary coated anode with 30% RhO_x. It means that the ternary coatings have the highest specific surface area. This result is in accordance with the CV curves and SEM micrographs (the observation of a cracked-mud morphology for these coatings). The capacitance of the ternary coatings was much higher than that of the coatings without RhO_x. These results are in accordance with De souza et al. [30] achievements about pseudo-capacitive behavior of Ti/RhO_x + Co_3O_4 electrodes.

To better understand the electrochemical behavior of the coatings, the EIS examinations were carried out on the specimens as a function of anodization time. As can be seen in Figs. 11–15, the semi-circle radius was dependent on the anodizing time in the low-frequency range at 1.35 $V_{vs\ SCE}$. Therefore, the charge transfer resistance at the active outer surface ($R_{ct,O}$) could be also depend on time. Moreover, by increasing the anodizing time, the charge transfer resistance was also raised. The Bode-phase plots (Figs. 11d–15d) revealed that the phase angle was increased at high frequency domain by time probably due to the growth of the middle layer (TiO_2). In contrast, the phase angle was reduced by increasing the anodizing time in the low-frequency regions, which can be related to the destruction of the active catalytic layer [9,10].

Anodic voltammetry charge (q^*_a) is considered as a direct measurement of the electrochemical active surface area [30]. As mentioned before, the decrease of q^*_a is due to the erosion or corrosion of the active dense layer. Therefore, if the wear of electrode's coating is accompanied by q^*_a reduction, $R_{ct,O}$ will be a function of the anodizing time, as displayed by the equation (3) [23]. Based on the section 3-4, it could be clearly seen that as the anodizing time was increased, the anodic voltammetry charge or the electrochemical active surface areas were decreased at an approximately constant rate.

$$R_{ct,O} = \frac{K}{q^*(t)} \quad (3)$$

According to the equation (3), the charge transfer resistance is enhanced by increasing electrolysis time. Experimentally, in the Nyquist diagrams obtained for different times, the length of the semi-circles was increased in the low-frequency ranges for the coatings with different compositions. According to the Table 5, after t = 0.5 t_{6V}, $R_{ct,O}$ remained almost constant for the specimens 55% IrO_2+15%RhO_x+30%ZrO_2 and 25%IrO_2+45%RhO_x+30%ZrO_2. However, for other electrodes, after this time and the end of the stability region, the charge transfer resistance was increased on the active outer surfaces. Typically, this phenomenon is the result of the selective dissolution of the active catalysts presented in the oxide coatings. However, the increase in the charge transfer resistance at the external active surface after the complete destruction of the anode and the deactivation of the electrode could be ascribed to the catalytic materials deficient in the oxide coatings, as well as the passivation of the titanium substrate [9,23].

In the electrodes with the high porosity/density ratio, the wear in the electrode is typically accompanied by a decrease in the actual surface area. Da Silva et al. [23] have shown that the dependence of $C_{dl,O}$ on the anodizing time is in accordance with the equation (4):

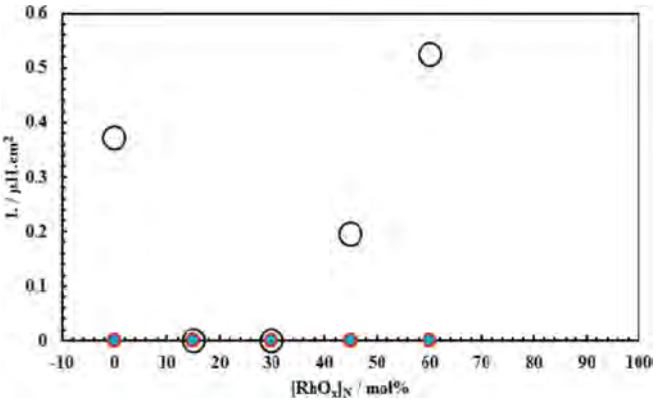

Fig. 16. Inductance dependence on electrolysis time and [RhO_x] in the 0.5 mol L^{-1} H_2SO_4 at the potential of 1.35 V_{SCE}, the unfilled circle: $t_1 = 0$, the red filled circle: $t_2 = 0.5t_{6v}$ and the blue filled circle: $t_3 = t_{6v}$.

Table 6
$C_{dl,I}$ and $C_{dl,O}$ values for all specimens were calculated using the equation (2) and the impedance parameters shown in Table 5.

Specimen No	t/s	$C_{dl,I}$/mF.cm^{-2}	$C_{dl,O}$/mF.cm^{-2}	Chi-squared
70%IrO_2 + 30%ZrO_2	0	0.00007	3.07	3.0×10^{-3}
	6000	0.01	0.41	4.1×10^{-3}
	12000	0.003	0.24	1.2×10^{-2}
55%IrO_2 + 15%RhO_x + 30%ZrO_2	0	1.02	6.10	8.7×10^{-3}
	8250	0.08	0.61	4.6×10^{-3}
	16500	0.003	0.01	3.3×10^{-3}
40%IrO_2 + 30%RhO_x + 30%ZrO_2	0	0.75	6.44	5.1×10^{-3}
	16500	0.007	0.60	1.3×10^{-2}
	33000	0.005	0.01	1.1×10^{-2}
25%IrO_2 + 45%RhO_x + 30%ZrO_2	0	0.44	5.46	7.9×10^{-3}
	18000	0.008	2.59	8.7×10^{-3}
	36000	0.005	0.11	4.1×10^{-3}
10%IrO_2 + 60%RhO_x + 30%ZrO_2	0	0.02	5.25	1.5×10^{-2}
	26250	0.007	2.69	9.0×10^{-3}
	52500	0.004	0.07	4.0×10^{-4}

$$C_{dl,O}(t) = K.A_G.(rf(t)) \quad (4)$$

where K is a constant, A_G is the geometric area of the electrode and rf is the roughness factor of the surface.

For all the MMO anodes, the capacitance of the double layer was reduced by increasing the anodizing time. It can be attributed to the wear and erosion of the coating's surface and the subsequent decrease of roughness in the surface. By comparison of the results of Tables 5 and 6, it can be concluded that the behavior of capacitance of the double layer (on the outer surface interface) with time was in a good agreement with the obtained values for $R_{ct,O}$.

However, changes in $C_{dl,O}$ vs time can be correlated with the active surface area and the number of active sites [9]. The amount of $C_{dl,O}$ was decreased by the increasing time. This phenomenon is related to the removal of the non-sticky oxide coating and the corrosion of the active dense layer. A sharp decline in $C_{dl,O}$, as compared to the initial values, indicated the inactivity of the anode. The values of n for the Q_{dl} constant phase element were between 0.55 and 0.75. The decrease in n values represented the process of electrolyte penetration into the inner surface of the coating over the electrolysis time. Further, the values of n for Q_f during the electrolysis time were between 0.60 and 0.94. The initial n values were as high as 0.6. This n value, which was calculated before the accelerated lifetime test, was related to the formation of the heterogeneous oxide layer at the coating/substrate interface or the formation of the non-stoichiometric $TiO_{(2-x)}$ middle layer [9]. Some researches believed that the increase in the n value could be due to the growth of the TiO_2 layer by oxidation [9]. It was also found that the growth of the oxide layer formed during the calcination process with the stoichiometric structure could be another reason for the increase in n value. In the work carried out by Audichon et al. [32], it was reported that increasing the n values up to 0.9 for the titanium electrode coated with $Ir_{0.3}Ti_{0.7}O_2$ could be due to the formation of TiO_2 dielectric layer in the substrate-coating interface. These results were in agreement with the significant increase in the TiO_2 intensity in the X-ray diffraction patterns after ALT (Fig. 5) [10,32].

Moreover, the data listed in Table 5 revealed that $R_{ct,I}$ was increased rapidly in all coatings due to the complete destruction of the coating and the initiation of the passivation process. Also, by increasing the electrolysis time and the growth of the TiO_2 insulation layer, the $C_{dl,I}$ value was decreased sharply [23].

The another point extracted from the data of Table 5 is that both $R_{ct,I}$ and $R_{ct,O}$ were increased after electrolysis, but, $R_{ct,I}$ showed a more significant increase than $R_{ct,O,}$ as compared to the initial values. Also, the addition of RhO_x increased the micro porosity level of the coatings and, thereby improved their charge transfer resistance at the active internal layer. In other words, penetration of the electrolyte in the micro-porosity of the coatings containing RhO_x promoted the formation of passive layer and a significant increase in the charge transfer resistance occurred due to the next thickening of the anodic layer throughout the interface region. It could be inferred that although the oxide coatings were worn and destroyed, the main mechanism for the destruction of the anode during the electrolysis time was not the dissolution of the oxide coating. In fact, in this case, the passivation of the Ti substrate was the main destruction mechanism [9]. In contrast, in the binary coating (Ti/70%IrO_2−30%ZrO_2), the lower increase in charge transfer resistance was due to the coating's dense nature. Also, in this case, less electrolyte could penetrate into the MMO bulk layer and a delay was occurred in the formation of the oxide layer. Therefore, the main reason for the deactivation of the Ti/70%IrO_2−30%ZrO_2 after anodizing was the further dissolution of the surface oxide layer. It is important to discuss about the presence of the inductive behavior observed in this work in accordance with the other researches in EIS examinations of rugged/porous electrodes [33]. The inductive behavior of different coatings as function of anodization time is shown in Fig. 16. Interestingly, the inductance value observed to be reduced by increasing the time. This trend can be ascribed to the reduction of active surface areas and enhancing the thickness of the intermediate layer of TiO_2 [23]. According to the data reported in Table 6, it was found that the inductance values of the coating without RhO_x and the coatings with 45% and 60% RhO_x were reduced by increasing the time. The changes in the chemical nature and the morphology of the oxide coating during anodizing were reported to be the main responsible factors for this behavior. The inductance values recorded for other coatings were near zero, evidencing the increase in the resistance ($R_{ct,O}$, and $R_{ct,I}$) over the anodizing time [23].

4. Conclusions

In this study, the effect of RhO_x concentration on the deactivation and corrosion behavior of Ti/IrO_2-RhO_x-ZrO_2 electrodes were investigated in 0.5 mol L^{-1} H_2SO_4 solution. The coatings were fabricated using thermal decomposition of a chlorine precursor mixture at 550 °C. The microstructural investigations revealed that a cracked muddy structure with smooth areas. By increasing the RhO_x molar percentage, more cracks were formed in the coating structure. ALT results clarified that the anode service life was dependent on the RhO_x molar percentage. Ti/10%IrO_2-60%RhO_x-30%ZrO_2 electrode had the highest service life and Ti/70%IrO_2−30% ZrO_2 electrode showed the lowest electrochemical stability. The CV results demonstrated a quasi-capacitance behavior for coatings and the amounts of voltammetry charge and the electrochemical active surface areas were increased by enhancing the RhO_x content. Further, with the lapse of electrolysis time, anodic voltammetry charge was decreased for the all specimens. The EIS results revealed that increasing the amount of RhO_x increased the charge transfer resistance of the outer active surfaces and decreased the ability of coatings for oxygen evolution. Also, the electrical conductivity of coatings was decreased by increasing the rhodium oxide. Furthermore, it was found that (the EIS examinations after ALT) the formation of TiO_2 passive layer at the interface of the substrate/oxides layer was the main destruction mechanism of the coated anodes. Finally, it was concluded that the anode with 10%IrO_2-60%RhO_x-30%ZrO_2 coating revealed larger electrochemically active surface area, higher stability and inferior electrocatalytic activity for oxygen evolution.

Acknowledgements

Dr. M. Shirani is acknowledged for experimental help and supports.

References

[1] W. Wu, Z.-H. Huang, T.-T. Lim, Recent development of mixed metal oxide anodes for electrochemical oxidation of organic pollutants in water, Appl. Catal. A Gen. 480 (2014) 58–78, https://doi.org/10.1016/j.apcata.2014.04.035.
[2] L. Xu, Y. Xin, J. Wang, A comparative study on IrO_2-Ta_2O_5 coated titanium electrodes prepared with different methods, Electrochim. Acta 54 (2009) 1820–1825, https://doi.org/10.1016/j.electacta.2008.10.004.
[3] F. Moradi, C. Dehghanian, Addition of IrO_2 to RuO_2+TiO_2 coated anodes and its effect on electrochemical performance of anodes in acid media, Prog. Nat. Sci. Mater. Int. 24 (2014) 134–141, https://doi.org/10.1016/j.pnsc.2014.03.008.
[4] Y. Xin, L. Xu, J. Wang, X. Li, Effect of sintering temperature on microstructure and electrocatalytic properties of Ti/IrO_2-Ta_2O_5 anodes by Pechini method, Xiyou Jinshu Cailiao Yu Gongcheng/Rare Met. Mater. Eng. 39 (2010).
[5] Z. Yan, H. Meng, Electrochemical investigation of the IrO_2-Ta_2O_5 coated anode with different heat treatment processes of the titanium substrates, Electrochem. Solid State Lett. 14 (2011) C16, https://doi.org/10.1149/1.3611016.
[6] J.J. Zhang, J.M. Hu, J.Q. Zhang, C.N. Cao, IrO_2-SiO_2 binary oxide films: geometric or kinetic interpretation of the improved electrocatalytic activity for the

oxygen evolution reaction, Int. J. Hydrogen Energy 36 (2011) 5218–5226, https://doi.org/10.1016/j.ijhydene.2011.01.131.
[7] L.K. Xu, J.D. Scantlebury, Electrochemical surface characterization of IrO_2-Ta_2O_5 coated titanium electrodes in Na_2SO_4 solution, J. Electrochem. Soc. 150 (2003) B288–B293.
[8] Z. Yan, Y. Zhao, Z. Zhang, G. Li, H. Li, J. Wang, Z. Feng, M. Tang, X. Yuan, R. Zhang, Y. Du, A study on the performance of IrO_2-Ta_2O_5 coated anodes with surface treated Ti substrates, Electrochim. Acta 157 (2015) 345–350, https://doi.org/10.1016/j.electacta.2015.01.005.
[9] S.M. Hoseinieh, F. Ashrafizadeh, M.H. Maddahi, A comparative investigation of the corrosion behavior of RuO_2–IrO_2–TiO_2 coated titanium anodes in chloride solutions, J. Electrochem. Soc. 157 (2010) E50, https://doi.org/10.1149/1.3294569.
[10] J.M. Hu, H.M. Meng, J.Q. Zhang, C.N. Cao, Degradation mechanism of long service life Ti/IrO_2-Ta_2O_5 oxide anodes in sulphuric acid, Corros. Sci. 44 (2002) 1655–1668, https://doi.org/10.1016/S0010-938X(01)00165-2.
[11] M. Goudarzi, M. Ghorbani, Deposition of (Ti,Ru)O_2 and (Ti,Ru,Ir)O_2 oxide coatings prepared by sol–gel method on titanium, J. Sol. Gel Sci. Technol. 79 (2016) 44–50.
[12] J. Bagchi, S.K. Bhattacharya, The effect of composition of Ni-supported Pt-Ru binary anode catalysts on ethanol oxidation for fuel cells, J. Power Sources 163 (2007) 661–670, https://doi.org/10.1016/j.jpowsour.2006.09.063.
[13] C. Deng, Monolayer dispersion thresholds and threshold effect displayed by supported catalysts, Front. Chem. China 3 (2008) 391–399, https://doi.org/10.1007/s11458-008-0084-2.
[14] M. ário, H.P. Santana, L.A. De Faria, J.F.C. Boodts, Investigation of the properties of Ti/[IrO_2-Nb_2O_5] electrodes for simultaneous oxygen evolution and electrochemical ozone production, EOP, Electrochim. Acta. 49 (2004) 1925–1935, https://doi.org/10.1016/j.electacta.2003.12.021.
[15] Y.-Q. Shao, Z.-Y. Yi, C. He, J.-Q. Zhu, D. Tang, Effects of annealing temperature on the structure and capacitive performance of nanoscale Ti/IrO_2-ZrO_2 electrodes, J. Am. Ceram. Soc. 98 (2015) 1485–1492, https://doi.org/10.1111/jace.13475.
[16] D. Rosestolato, J. Fregoni, S. Ferro, A. De Battisti, Influence of the nature of the electrode material and process variables on the kinetics of the chlorine evolution reaction. the case of IrO_2-based electrocatalysts, Electrochim. Acta 139 (2014) 180–189, https://doi.org/10.1016/j.electacta.2014.07.037.
[17] M.J. Klink, M.E. Makgae, A.M. Crouch, Physico-chemical and electrochemical characterization of Ti/RhO_x–IrO_2 electrodes using sol–gel technology, Mater. Chem. Phys. 124 (2010) 73–77, https://doi.org/10.1016/j.matchemphys.2010.05.016.
[18] L.L. Swette, A.B. LaConti, S.A. McCatty, Proton-exchange membrane regenerative fuel cells, J. Power Sources 47 (1994) 343–351.
[19] A. Hrussanova, E. Guerrini, S. Trasatti, Thermally prepared Ti/RhO_x electrodes IV: O_2 evolution in acid solution, J. Electroanal. Chem. 564 (2004) 151–157.
[20] B. Liu, S. Wang, C. Wang, Y. Chen, B. Ma, J. Zhang, Surface morphology and electrochemical properties of RuO_2-doped Ti/IrO_2-ZrO_2 anodes for oxygen evolution reaction, J. Alloy. Comp. 778 (2019) 593–602, https://doi.org/10.1016/j.jallcom.2018.11.191.
[21] X. Qin, F. Gao, G. Chen, Effects of the geometry and operating temperature on the stability of Ti/IrO_2-SnO_2-Sb_2O_5 electrodes for O_2 evolution, J. Appl. Electrochem. 40 (2010), https://doi.org/10.1007/s10800-010-0154-2.
[22] Y. Duan, Q. Wen, Y. Chen, T. Duan, Y. Zhou, Preparation and characterization of TiN-doped Ti/SnO_2-Sb electrode by dip coating for Orange II decolorization, Appl. Surf. Sci. 320 (2014) 746–755, https://doi.org/10.1016/j.apsusc.2014.09.182.
[23] L.M. Da Silva, K.C. Fernandes, L.A. De Faria, J.F.C. Boodts, Electrochemical impedance spectroscopy study during accelerated life test of conductive oxides: Ti/(Ru + Ti + Ce)O_2-system, Electrochim. Acta 49 (2004) 4893–4906, https://doi.org/10.1016/j.electacta.2004.05.043.
[24] L. Popa, E. Guerrini, S. Trasatti, Effect of composition on the surface and electrocatalytic properties of Ti/IrO_x + RhO_x electrodes: H_2 evolution from acidic solution, J. Appl. Electrochem. 35 (2005) 1213–1223.
[25] L.A. da Silva, V.A. Alves, M.A.P. da Silva, S. Trasatti, J.F.C. Boodts, Morphological, chemical, and electrochemical properties of Ti/(TiO_2 + IrO_2) electrodes, Can. J. Chem. 75 (1997) 1483–1493.
[26] Y.E. Roginskaya, O.V. Morozova, G.I. Kaplan, R.R. Shifrina, M. Smirnov, S. Trasatti, Thermally prepared Ti/RhO_x electrodes-I structural, electronic and surface properties, Electrochim. Acta 38 (1993) 2435–2441, https://doi.org/10.1016/0013-4686(93)85113-D.
[27] L.K. Xu, J.D. Scantlebury, A study on the deactivation of an IrO_2-Ta_2O_5 coated titanium anode, Corros. Sci. 45 (2003) 2729–2740, https://doi.org/10.1016/S0010-938X(03)00108-2.
[28] K.R.W.Richard G. Compton, Eduardo Laborda, Understanding Voltammetry: Simulation of Electrode Processes, World Scientific, 2014, https://doi.org/10.1142/p910.
[29] P.M. De Campos, A.V. Benedetti, L.A. De Faria, V. Cardoso, J.F.C. Boodts, Structural and surface properties of thermally prepared Ti/$Rh_xTi_{(1-x)}O_y$ electrodes: I - influence of preparation parameters, Electrochim. Acta 47 (2002) 1283–1295, https://doi.org/10.1016/S0013-4686(01)00800-3.
[30] A.R. De Souza, E. Arashiro, H. Golveia, T.A.F. Lassali, Pseudocapacitive behavior of Ti/RhO_x+Co_3O_4 electrodes in acidic medium: application to supercapacitor development, Electrochim. Acta 49 (2004) 2015–2023, https://doi.org/10.1016/j.electacta.2003.12.031.
[31] L.M. Da Silva, L.A. De Faria, J.F.C. Boodts, Electrochemical impedance spectroscopic (EIS) investigation of the deactivation mechanism, surface and electrocatalytic properties of Ti/RuO_2(x)+Co_3O_4(1-x) electrodes, J. Electroanal. Chem. 532 (2002) 141–150, https://doi.org/10.1016/S0022-0728(02)00810-0.
[32] T. Audichon, E. Mayousse, S. Morisset, C. Morais, C. Comminges, T.W. Napporn, K.B. Kokoh, Electroactivity of RuO_2-IrO_2 mixed nanocatalysts toward the oxygen evolution reaction in a water electrolyzer supplied by a solar profile, Int. J. Hydrogen Energy 39 (2014) 16785–16796, https://doi.org/10.1016/j.ijhydene.2014.07.170.
[33] L.A. da Silva, V.A. Alves, M.A.P. da Silva, S. Trasatti, J.F.C. Boodts, Electrochemical impedamce, SEM, EDX and voltammetric study of oxygen evolution on Ir+ Ti+ Pt ternary oxide electrodes in alkaline solution, Electrochim. Acta 41 (1996) 1279–1285.